DESY 94-117

Comparison of energy flows in deep inelastic scattering events with and without a large rapidity gap

ZEUS Collaboration

August 18, 1994

Abstract

Energy flows in deep inelastic electron-proton scattering are investigated at a centre-of-mass energy of 296 GeV for the range $Q^2 \geq 10$ GeV^2 using the ZEUS detector. A comparison is made between events with and without a large rapidity gap between the hadronic system and the proton direction. The energy flows, corrected for detector acceptance and resolution, are shown for these two classes of events in both the HERA laboratory frame and the Breit frame. From the differences in the shapes of these energy flows we conclude that QCD radiation is suppressed in the large-rapidity-gap events compared to the events without a large rapidity gap.

1 Introduction

In a previous publication [1] we reported the observation of events with a large rapidity gap in deep inelastic ep scattering (DIS) at HERA. We concluded that these events are not described by standard QCD-inspired fragmentation models [2, 3]. Furthermore we presented indications that the mechanism is diffractive, leading twist and consistent with the exchange of a colourless object, generically called the pomeron. Recently we have also reported on the observation of jet production in these events [4].

Energy flow measurements naturally complement jet studies; in particular, they are sensitive to QCD radiation, i.e. soft partonic emissions in addition to the hard scattering. Energy flows do not depend on a particular jet classification scheme, they are infrared-safe and, according to the idea of local parton-hadron duality (LPHD) [5], they are determined by the partonic structure of the events. Experimentally in the ZEUS detector at HERA, energy flows have the advantage that they can be measured with little bias in a large fraction of the events. In a previous publication [6] we have used energy flow measurements to discriminate between different QCD-inspired models for DIS. In this paper we study the hadronic energy flow in large-rapidity-gap events, both in the laboratory and in the Breit frames of reference. We also compare with the corresponding energy flows in non-rapidity-gap events.

2 Experimental setup

2.1 HERA machine conditions

The experiment was performed at the electron-proton collider HERA using the ZEUS detector. During 1993 HERA operated with bunches of electrons of energy $E_e = 26.7$ GeV colliding with bunches of protons of energy $E_p = 820$ GeV, with a time between bunch crossings of 96 ns. HERA is designed to run with 210 bunches in each of the electron and proton rings. For the 1993 data taking 84 paired bunches were filled for each beam and in addition 10 electron and 6 proton bunches were left unpaired for background studies. The electron and proton beam currents were typically 10 mA.

2.2 The ZEUS detector

ZEUS is a multipurpose magnetic detector whose configuration for the 1992 running period has been described elsewhere [7, 8]. Here we give a brief description concentrating on those parts of the detector relevant for the present analysis and those which were different for the 1993 running.

Charged particles are tracked by the inner tracking detectors which operate in a magnetic field of 1.43 T provided by a thin superconducting coil. Immediately surrounding the beampipe is the vertex detector (VXD), a cylindrical drift chamber which consists of 120 radial cells, each with 12 sense wires. It uses a slow drift velocity gas (dimethylether) [9] and the presently achieved resolution is 50 μm in the central region of a cell and 150 μm near the edges. Surrounding the VXD is the central tracking detector (CTD) which consists of 72 cylindrical drift chamber

layers, organised into 9 'superlayers' [10]. With the present understanding of the chamber and the reconstruction software, a spatial resolution of ~ 280 μm has been achieved. In events with charged particle tracks, using the combined data from both chambers, resolutions of 0.6 cm in Z and 0.1 cm in radius in the XY plane[1] are obtained for the primary vertex reconstruction. From gaussian fits to the Z vertex distribution, the rms spread is found to be 10.5 cm in agreement with the expectation from the proton bunch length.

The solenoid is surrounded by a high-resolution uranium-scintillator calorimeter divided into three parts, forward (FCAL) covering the pseudorapidity[2] region $4.3 \geq \eta \geq 1.1$, barrel (BCAL) covering the central region $1.1 \geq \eta \geq -0.75$ and rear (RCAL) covering the backward region $-0.75 \geq \eta \geq -3.8$. Holes of 20×20 cm^2 in the centre of FCAL and RCAL are required to accommodate the HERA beam pipe. The resulting solid angle coverage is 99.7% of 4π. The calorimeter parts are subdivided into towers which in turn are subdivided longitudinally into electromagnetic (EMC) and hadronic (HAC) sections. The sections are subdivided into cells, each of which is viewed by two photomultiplier tubes. The calorimeter is described in detail in [11, 12, 13].

The C5 beam monitor, a small lead-scintillator counter arrangement, located at $Z = -3.2$ m close to the beampipe, was used to detect upstream proton beam interactions and to measure the timing and longitudinal structure of the proton and electron bunches from the arrival time of stray particles accompanying the particle bunches in HERA. The vetowall detector, consisting of two layers of scintillator on either side of an 87 cm thick iron wall centered at $Z = -7.3$ m was also used to tag off-beam background particles.

For measuring the luminosity as well as for tagging very small Q^2 processes, we use two lead-scintillator calorimeters [14]. Bremsstrahlung photons emerging from the electron-proton interaction point (IP) at angles $\theta_\gamma \leq 0.5$ mrad with respect to the electron beam axis hit the photon calorimeter at 107 m from the IP. Electrons emitted from the IP at scattering angles less than or equal to 6 mrad and with energies $0.2E_e < E'_e < 0.9E_e$ are deflected by beam magnets and hit the electron calorimeter placed 35 m from the IP.

2.3 Trigger conditions

Data were collected with a three level trigger [7]. The First Level Trigger (FLT) is built as a deadtime-free pipeline. The FLT for DIS events required a logical OR of three conditions on sums of energy in the EMC calorimeter cells: either the BCAL EMC energy exceeded 3.4 GeV; or the RCAL EMC energy, excluding the towers immediately adjacent to the beam-pipe, exceeded 2.0 GeV; or the RCAL EMC energy, including the beam-pipe towers, exceeded 3.75 GeV. For events with the scattered electron detected in the calorimeter, the FLT was essentially independent of the DIS hadronic final state. The FLT acceptance was greater than 97% for $Q^2 > 10$ GeV^2.

The Second Level Trigger (SLT) used information from a subset of detector components to differentiate physics events from backgrounds. The SLT rejected proton beam-gas events according to the event times measured in the rear calorimeter thereby reducing the FLT DIS triggers by an order of magnitude, but without loss of DIS events.

[1] The ZEUS coordinate system is defined as right-handed with the Z axis pointing in the proton beam direction, hereafter referred to as forward, and the X axis horizontal, pointing towards the centre of HERA.

[2] The pseudorapidity η is defined as $-\ln(\tan\frac{\theta}{2})$, where the polar angle θ is taken with respect to the proton beam direction from the nominal interaction point.

The Third Level Trigger (TLT) had available the full event information on which to apply physics-based filters. The TLT applied stricter cuts on the event times and also rejected beam-halo muons and cosmic muons. Events remaining after the above veto cuts were selected for output by the TLT if $\delta \equiv \Sigma_i E_i(1-\cos\theta_i) > 20\text{GeV} - 2E_\gamma$, where E_i, θ_i are the energy and polar angle (with respect to the nominal IP) of calorimeter cells and E_γ is the energy measured in the photon calorimeter of the luminosity monitor. For fully contained events $\delta \sim 2E_e = 53.4$ GeV. For events from photoproduction the scattered electrons remain in the rear beam pipe, and, due to the soft bremsstrahlung spectrum, δ peaks at low values.

3 Kinematics of deep inelastic scattering

The kinematic variables used to describe deep inelastic scattering events

$$e\ (k)\ +\ p\ (P) \rightarrow e\ (k')\ +\ anything \tag{1}$$

are the following: the negative of the squared four–momentum transfer carried by the virtual photon[3], $\gamma^\star$,

$$Q^2 = -q^2 = -(k-k')^2, \tag{2}$$

where k and k' are the four–momenta of the initial and final state electrons, respectively; the Bjorken variable

$$x = \frac{Q^2}{2q\cdot P} = \frac{Q^2}{ys}\ , \tag{3}$$

where P is the four–momentum of the incoming proton and s is the centre-of-mass energy squared of the ep system; the variable which describes the energy transfer to the hadronic final state

$$y = \frac{q\cdot P}{k\cdot P}\ ; \tag{4}$$

and W, the centre-of-mass energy of the $\gamma^\star p$ system,

$$W^2 = (q+P)^2 = \frac{Q^2(1-x)}{x} + M_p^2 \tag{5}$$

with M_p, the proton mass.

The kinematic variables, only two of which are independent, can be determined from the leptonic system, the hadronic system, or from both. Studies of the HERA kinematics have shown that it is advantageous, for the present analysis, to use the so-called *double-angle* method [15]. Quantities determined in this way will be denoted by the subscript DA. Here, all event variables are derived from the scattering angle of the electron and the angle γ_H. In the naïve Quark-Parton Model (QPM), γ_H corresponds to the scattering angle of the massless struck

[3]In the Q^2 range covered in this analysis, ep interactions are described to sufficient accuracy by the exchange of a virtual photon.

quark (leading to the current jet). It is determined from the measured energy depositions in the calorimeter cells in the following way: first the variables δ_H and y_{JB}[4] are determined from

$$\delta_H = \sum_i (E_i - p_{iZ}), \tag{6}$$

$$y_{JB} = \frac{\delta_H}{2E_e}. \tag{7}$$

The sum runs over all calorimeter cells i, excluding those assigned to the scattered electron, p_{iZ} is the Z component of a momentum vector $p_i = (E_i, p_{iX}, p_{iY}, p_{iZ})$ assigned to each cell i of energy E_i such that $p_i^2 = 0$. The variable y_{JB} is a good estimator for y even if a significant amount of energy escapes in the direction of the proton beam: final state particles produced close to this direction give a negligible contribution to δ_H, and therefore to y_{JB}, since these particles have $(E - p_Z) \sim 0$. Next, we calculate the transverse momentum, p_T, of the hadronic system and γ_H from

$$p_T^2 = \left(\sum_i p_{iX}\right)^2 + \left(\sum_i p_{iY}\right)^2, \tag{8}$$

$$\cos\gamma_H = \frac{{p_T}^2 - {\delta_H}^2}{{p_T}^2 + {\delta_H}^2}. \tag{9}$$

The pseudorapidity corresponding to the γ_H direction, η_{γ_H}, can be expressed as

$$\eta_{\gamma_H} = \ln\frac{p_T}{\delta_H}. \tag{10}$$

Complete formulae to calculate the double-angle quantities are given in [15]. Since p_T is related to Q and y through

$$p_T = Q \cdot \sqrt{1-y}, \tag{11}$$

one sees from the above formulae that if y is sufficiently high (> 0.04), γ_H will point into the rear hemisphere at low Q^2 ($Q^2 \sim 5$ GeV^2). As Q^2 grows the γ_H direction turns slowly to the forward hemisphere.

Energy flow distributions will also be presented in the Breit frame. The Breit frame is defined by the requirement that the vector $(q + 2xP)$ has no space-like components. As a consequence the virtual photon, $\gamma^\star$, carries only a space-like component, conventionally assigned to the negative z direction: $q = (0, 0, 0, -Q)$. The four-momentum of the proton, neglecting its mass, is then given by $P = (Q/2x, 0, 0, Q/2x)$. In the QPM, the interacting quark from the proton carries a momentum $p = xP$. The z component of the momentum of the incoming quark is $Q/2$ before and $p_z^{QPM} = -Q/2$ after the interaction with the $\gamma^\star$. The Breit frame is also referred to as the "brick wall" frame since in lowest order the incoming parton simply reverses its direction.

[4]The abbreviation JB stands for Jacquet–Blondel[16].

4 Data selection

The offline selection of DIS events was similar to that described in our earlier publications [1, 17]. Scattered electron candidates were selected by using the pattern of energy deposition in the calorimeter. The electron energy was required to be more than 10 GeV. The electron identification algorithm was tuned for purity rather than efficiency. In studies with Monte Carlo DIS events and test beam samples the purity was estimated to be ≥ 96 %. We demanded

- $Q^2_{DA} \geq 10$ GeV^2;
- $y_{JB} \geq 0.04$, to give sufficient accuracy for DA reconstruction;
- $\delta \geq 35$ GeV, to control radiative corrections and photoproduction background;
- $y_e \leq 0.95$, where y_e is the variable y defined in equation (4) calculated from the electron variables, to reduce the photoproduction background.

Furthermore we required

- a vertex, determined from VXD and CTD tracks, in the range $-50 \leq Z_{vtx} \leq 40$ cm and a radial distance from the beamline $R = \sqrt{X^2_{vtx} + Y^2_{vtx}} < 8.5$ cm;
- the position (X, Y) of the scattered electron in the RCAL to lie outside a square of 32×32 cm^2 centered on the beam axis;
- no more than 5 GeV of energy deposition in the photon calorimeter of the luminosity detector, to exclude events with large initial-state radiation.

Finally, we rejected Compton scattering events and cosmic and beam-related muons.

A total of 26210 events was selected in this way corresponding to an integrated luminosity of 550 nb^{-1}. Fig. 1(a) shows the distribution of the variable η_{max} for all events in the final selection where η_{max} is the pseudorapidity of the most forward calorimeter condensate with an energy above 400 MeV. A condensate is a contiguous energy deposit above 100 MeV for pure EMC and 200 MeV for HAC or mixed energy deposits. The distribution has not been corrected for detector acceptance and resolution and, in particular, the dip near $\eta_{max} \sim 1$ is a detector effect. Values of $\eta_{max} \geq 4.3$, which are outside the calorimeter acceptance, occur when energy is deposited in many contiguous cells around the beam pipe in the proton direction. Also shown in Fig. 1(a) are the results from two Monte Carlo programs, namely CDMBGF (full histogram) which describes standard DIS processes and POMPYT (dashed histogram) which is a model for diffractive DIS processes. The Monte Carlo programs are described in the following section. The normalizations of the Monte Carlo distributions have been chosen such that their sum gives an optimal description of the data. As noted in [1, 4, 18], the data show a clear excess over the predictions of a standard DIS model at values of $\eta_{max} < 1.5$. The event sample is split into two classes: those events which have $\eta_{max} < 1.5$ are called large-rapidity-gap events. The rest of the events are called non-rapidity-gap events. In total, 1241 events are in the first class and 24969 events are in the second class. For the large-rapidity-gap events an upper limit of 2% (25 events) was estimated for non-DIS backgrounds such as photoproduction, cosmics, beam-gas and beam-wall interactions.

We will compare energy flows with respect to the γ_H direction in large-rapidity-gap and in non-rapidity-gap events. For events selected by the η_{max} cut, the energy flow is necessarily small at pseudorapidities greater than η_{max}. In order to obtain a range of at least two units in pseudorapidity between η_{max} and η_{γ_H} we require $\eta_{\gamma_H} < -0.5$. A lower cut on η_{γ_H} was chosen at -2.5 units in order to avoid the boundary of the calorimeter near the rear beam pipe. The centre of the γ_H bin, $\eta_{\gamma_H} = -1.5$, corresponds to $\gamma_H = 155^o$. In Fig. 1(b) the two curves delimit the range $-2.5 < \eta_{\gamma_H} < -0.5$. The horizontal lines delimit the Q^2_{DA} bins used in the analysis. The highest Q^2_{DA} bin has no upper limit. We see from this figure that the majority (79%) of the large-rapidity-gap events with $Q^2_{DA} > 10$ GeV^2 are contained in the selected intervals. Applying the same cuts to the non-rapidity-gap events we select 51% of the sample as shown in Fig. 1(c).

5 The Monte Carlo simulation

The expected final states from DIS were modelled using two different sets of generators, the first one for the description of the non-rapidity-gap events and the second one to model the large-rapidity-gap events.

Events from standard DIS processes were generated using two alternative Monte Carlo models, LEPTO 6.1 [19] with ARIADNE 4.0 [20, 2] as implemented in [21](CDMBGF) and with the matrix element plus parton showers (MEPS) option within LEPTO 6.1. In both models electroweak radiative corrections were implemented with the help of HERACLES [22] which was interfaced to LEPTO 6.1 via the program DJANGO 6.0 [23]. The proton parton densities were chosen to be the MRSD$-'$ set [24] which gives an adequate description of the HERA structure function results [17, 25]. Note that these Monte Carlo codes do not contain explicit contributions from diffractive $\gamma^\star p$ interactions.

In order to model the DIS hadronic final states from large-rapidity-gap events we have studied two Monte Carlo event samples, one of which was generated by POMPYT [26]. POMPYT is a Monte Carlo realisation of factorisable models for high energy diffractive processes, where within the PYTHIA [27] framework, the beam proton emits a pomeron, whose constituents take part in a hard scattering process with the virtual photon. The quark density in the pomeron is assumed to be hard:

$$P(\beta) = constant \cdot \beta(1-\beta) \tag{12}$$

where β denotes the fraction of the pomeron momentum carried by the quark. Note that the shape of the hard quark density in POMPYT is the same as that proposed by Donnachie and Landshoff [28]. The second sample was generated following the Nikolaev-Zakharov (NZ) model [29] which was interfaced to the Lund fragmentation scheme [30]. The NZ model, which is not factorisable, assumes that the exchanged virtual photon fluctuates into a quark-antiquark pair which interacts with a colourless two-gluon system emitted by the incident proton. The resulting effective β distribution is somewhat softer than the one used for POMPYT. The diffractive Monte Carlo samples were generated with parameter settings as described in [4]. QED radiative processes were not simulated for these events. With the DIS selection cuts of section 4, radiative corrections are below 10% [17]. Event samples generated by Monte Carlo methods were processed by the ZEUS detector simulation program which is based on GEANT 3.13 [31] and which incorporates detector and trigger simulation. The events were then run through the standard ZEUS offline reconstruction program.

6 Correction procedure

In the HERA frame we measure the energy flow, $1/N \cdot dE/d(\Delta\eta)$, as a function of the pseudorapidity difference $\Delta\eta = \eta_{cell} - \eta_{\gamma_H}$. The energy flow is determined from all calorimeter cells with energies above 60 (110) MeV for EMC (HAC) cells. The pseudorapidity, η_{cell}, is calculated from the angle between the proton direction and a line connecting the measured vertex and the geometric centre of the cell. In the Breit frame, we measure $1/N \cdot dE/d(\eta^\star)$ as a function of $\eta^\star$, the pseudorapidity of a condensate in the Breit frame.

The measured distributions are distorted with respect to those of the true final state particles due to trigger biases, event selection cuts and the finite acceptance and the response of the detector. The detector and trigger simulation programs together with samples generated from different Monte Carlo programs have been used to estimate the distortions and to correct for them by multiplying the measured distributions by a correction function $c(\chi)$ in each bin of Q^2_{DA} and γ_H. χ is either the pseudorapidity difference, $\Delta\eta$, or the pseudorapidity in the Breit frame, $\eta^\star$, and $c(\chi)$ is calculated in the simulation as the bin-by-bin ratio

$$c(\chi) = \left(\frac{1}{N_{gen}}\frac{\Delta E(\chi)_{gen}}{\Delta\chi}\right) \Big/ \left(\frac{1}{N_{obs}}\frac{\Delta E(\chi)_{obs}}{\Delta\chi}\right). \tag{13}$$

In this expression variables with subscript (gen) and (obs) refer to the true quantities as generated in the Monte Carlo program at the hadron level and the simulated quantities observed at the detector level, respectively. N_{gen} and N_{obs} are the number of events generated and observed in the respective (γ_H, Q^2_{DA}) bins, $\Delta E_{gen}(\Delta E_{obs})$ is the sum over the generated (observed) energies of hadrons (calorimeter cells) in the respective bins of χ, and $\Delta\chi$ is the width of the χ bin. Thus one accounts for energy losses, resolution, event selection cuts, event migrations and trigger biases. We correct the non-rapidity-gap event sample using the CDMBGF Monte Carlo program and the large-rapidity-gap events using the POMPYT Monte Carlo program for diffractive $\gamma^\star p$ scattering.

To confirm that this correction method is justified we have checked that

- the chosen bins in $\Delta\eta$ and $\eta^\star$ are at least 30% larger than the resolution;
- the correction function $c(\chi)$ does not deviate from unity by more than 40 % in the bins shown;
- $c(\chi)$ does not show a strong model-dependence in models that adequately describe the data. The differences between the Monte Carlo models are treated as part of the systematic error.

However, no correction is made to the large-rapidity-gap data for the η_{max} cut which is used to define this sample. The acceptance due to the η_{max} cut for events generated using the diffractive Monte Carlo programs is about 35%. Therefore in this sample a cut equivalent to the η_{max} cut is applied at the generator level by excluding events with hadrons above 400 MeV in the range $1.5 \leq \eta \leq 5$. The value of $\eta = 5$ was chosen to approximate the edge of the forward beam pipe aperture in the calorimeter.

We estimate the systematic errors by:

- using different Monte Carlo models;
- choosing a different electron identification algorithm;
- varying the η_{max} cut between 1.5 and 1.8;
- varying the cut on δ between 35 and 40 GeV;
- varying the energy scale of the calorimeter by $\pm 5\%$;
- moving the Z vertex position by ± 1 cm.

The chosen variations are consistent with our present knowledge of the detector performance. The contributions of the above effects to the systematic error have been added in quadrature. The dominant source of systematic error is the model dependence at about 20 %.

7 Results

The energy flow $1/N \cdot dE/d(\Delta\eta)$, corrected as described above, is shown in Fig. 2 as a function of $\Delta\eta = \eta_{cell} - \eta_{\gamma_H}$. The average Q^2_{DA} varies from 14 GeV^2 in Fig 2(a) to 380 GeV^2 in Fig 2(e). In all of the comparisons cells in the very forward region with $\eta_{cell} > 2.5$ (corresponding to $\theta < 10^o$) were removed to reduce model and measurement uncertainties. The effect of this cut on the uncorrected energy flow for $10 < Q^2 < 20$ GeV^2 is shown in Fig. 1(d). The solid circles depict the energy flow as a function of $\Delta\eta$ for all calorimeter cells, while in the histogram cells with $\eta_{cell} > 2.5$ have been removed. As can be seen the cut influences the energy flow only in the region $\Delta\eta \geq 3$. The energy flows of the selected large-rapidity-gap events are not influenced by this cut.

7.1 Energy flows in the laboratory frame

We first discuss the energy flow of the non-rapidity-gap events (open circles in Fig. 2). At high Q^2_{DA} the QPM peak appears near $\Delta\eta \sim 0$. Furthermore, the energy flow rises towards the proton direction and there is substantial energy flow in between the struck quark and proton directions. With decreasing Q^2_{DA}, the QPM peak becomes less pronounced. At low Q^2_{DA} it is clearly seen that the QPM peak is rather broad, and is shifted towards positive values of $\Delta\eta$ by about 0.4 units and that the energy is emitted predominantly at positive values of $\Delta\eta$ [6]. The resolution in $\Delta\eta$ is approximately constant at 0.16 units over the entire range shown, determined predominantly by the resolution in η_{cell}.

The energy flow distributions of the large-rapidity-gap events (solid circles in Fig. 2) exhibit striking differences to the ones in the non-rapidity-gap events. In particular, the large-rapidity-gap-events show a much simpler structure:

- the peak of the energy flow is nearly centered at $\Delta\eta$=0;
- the energy is well collimated within ± 1 unit of pseudorapidity around the γ_H direction;

- the collimation changes little with Q^2_{DA};
- there is only little energy flow in the region between the γ_H and the proton directions.

We explain the differences of the two energy flow distributions by the suppression of QCD radiation in the large-rapidity-gap events. In the naïve QPM the photon strikes a quark, with momentum fraction xP in the proton, and produces a massless jet. In contrast, in the leading order QCD correction to this process, the γ^* interacts with a parton from the proton and produces a quark-antiquark or quark-gluon pair. At the same value of x the incoming parton now carries a fraction ξ of the proton momentum $p = \xi P$ where ξ is larger than x to allow for the emission of a parton pair with, in general, a non-zero invariant mass[5]. This leads to a net shift of the resultant direction of the parton pair towards the proton direction.

To estimate the size of the effect, we have computed the contribution to the energy flow from just the first order QCD processes. We have used the exact first order matrix element (ME) calculation for QCD Compton (QCDC) and Boson-Gluon Fusion (BGF) as implemented in the LEPTO 6.1 Monte Carlo program [19]. The contributions of the two final-state partons to the energy flow are shown in Fig. 3 for two (x, Q^2) intervals. The computation at the parton level, with the standard ME cutoff parameter setting, confirms the qualitative argument developed above: the radiation is emitted strongly in the direction of the proton with a flat distribution in between the proton remnant and the QPM peak. The peak is also shifted at low Q^2 towards the proton direction. The characteristics of the first order processes are preserved in higher order since the emission of three, four and more partons can be approximated by a Markov chain of emissions where each individual emission has the same structure as in the two parton case [32].

The CDMBGF Monte Carlo calculation which includes higher order partonic emissions (full histogram in Fig. 2) is in good quantitative agreement with the non-rapidity-gap data (open circles in Fig. 2). Hence, we can conclude that QCD radiation is responsible for shifting the QPM peak and for filling in the region between the struck quark and proton directions. Reversing the argument we can also conclude that QCD radiation must be suppressed in the large-rapidity-gap events, otherwise we would observe both a shift of the QPM peak towards the proton direction and substantially more energy emitted between the direction γ_H and the proton. A very small fraction of the events generated using the CDMBGF Monte Carlo program satisfy the η_{max} cut as can be seen in Fig. 1(a). The energy flows of these events (not shown here) are qualitatively similar to those of the large-rapidity-gap events indicating that by the η_{max} cut we select events with little QCD radiation also in the CDMBGF Monte Carlo sample. These events are the result of rare fluctuations in the parton showering process. Since we cannot reproduce the rate of large-rapidity-gap events observed in the data with standard DIS Monte Carlo models we compare the events to models for diffractive ep scattering. One of these models, namely POMPYT, is shown as the dashed histogram in Fig. 2. It is in good quantitative agreement with the data.

In our previous publications [1, 4] we have noted that in large-rapidity-gap events the mass M_X of the hadronic system observed in the detector is small compared to the typical masses observed in non-rapidity-gap events. The prominent features of the energy flow of the large-rapidity-gap events, namely the absence of a QPM peak shift and the narrow collimation, can

[5] Note that $(q + xP)^2 \equiv 0$ whereas $(q + \xi P)^2 > 0$.

be interpreted as a direct consequence of the fact that M_X is small in these events. Indeed, QCD radiation produces large masses, so that the observation of predominantly small masses M_X would lead to the same basic conclusion, namely that QCD radiation is suppressed.

7.2 Energy flows in the Breit frame

The structure of the energy flows in the HERA frame is dominated by the large transverse boost with respect to the virtual photon direction. In photon-aligned frames this kinematic effect is removed and the QCD dynamics become more apparent. In Fig. 4 we show the energy flow for the two classes of events as a function of the pseudorapidity, $\eta^\star$, in the Breit frame (see section 3). This frame is a photon-aligned frame and, as shall be shown later, it is a reasonable approximation to the centre-of-mass system of the diffractively produced hadrons in the large-rapidity-gap events.

These distributions were calculated in the following way: the transformation from the HERA frame to the Breit frame consists of a boost, followed by a rotation such that after the transformation the virtual photon direction is defined to be the z axis. The boost and rotation are computed from the momenta of the virtual photon and the incoming proton. The momentum of the virtual photon is determined by measuring the scattering angle of the electron in the calorimeter and determining its energy from the double-angle variables. This method minimizes the systematic error introduced by the transformation. A calorimeter condensate is treated as a particle with a pion mass. (The results obtained are not sensitive to the precise choice of this mass.) Its momentum is transformed into the Breit frame and the energy flow is plotted as a function of the pseudorapidity, $\eta^\star$. The distributions are corrected for the effects of detector acceptance and resolution. The corrections are smaller than 40 % in the range $-2 < \eta^\star < 2$ and the resolution in $\eta^\star$ varies from 0.1 units in the central region to 0.3 units at $\pm$ 2 units of pseudorapidity.

In the Breit frame one can separate the target and the current fragmentation regions. In Fig. 4 the current fragmentation region is on the left (negative values of $\eta^\star$) and the target fragmentation region is on the right (positive values of $\eta^\star$). In the non-rapidity-gap events the energy flow is steeply rising from the current region to the target region while in the large-rapidity-gap events it is flat at a value of the order of 1 GeV per unit of pseudorapidity. Hence in the target region the energy flow for large-rapidity-gap events is much smaller than for non-rapidity-gap events. In the current region, however, the energy flow for large-rapidity-gap events is larger than for non-rapidity-gap events.

This difference in the current fragmentation region is another sign of QCD radiation in the non-rapidity-gap events as can be seen from the following argument. In the QPM in the Breit frame the incoming quark carries momentum $Q/2$ and is emitted with momentum $p_z^{QPM} = -Q/2$ along the z direction. In the leading order QCD correction to the QPM the parton comes in with momentum $Q/2$, but the outgoing parton pair has a z component p_z^{rad} given by

$$p_z^{rad} = \frac{Q}{2}\left(\frac{\hat{s} - Q^2}{Q^2}\right) \tag{14}$$

where $\hat{s}$ is the square of the invariant mass of the emitted quark-antiquark or quark-gluon pair. When $Q^2 \gg \hat{s}$ the radiation is emitted in the QPM direction, $p_z^{rad} \sim p_z^{QPM}$. However,

at low Q^2, $\hat{s}$ is likely to be bigger than Q^2 and the radiation will be emitted in the direction opposite to the QPM direction. Typically, the minimum $\hat{s}$ is around 20 GeV^2 in our kinematic region, therefore at Q^2 around 10 GeV^2 the emitted radiation has $p_z^{rad} = Q/2$ or more, whereas $p_z^{QPM} = -Q/2$. QCD radiation pulls energy from the Breit frame current region into the target region. These features are well described by the CDMBGF Monte Carlo (solid histogram in Fig. 4).

The energy flows of the large-rapidity-gap events in the Breit frame are well described by the POMPYT Monte Carlo program with a hard structure function (dashed histogram in Fig. 4) and by the model of Nikolaev and Zakharov (dotted histogram in Fig. 4). The shaded histogram in Fig. 4 shows the contribution from the target hemisphere of the centre-of-mass system of the diffractively produced hadrons as calculated in the POMPYT Monte Carlo model. Within the framework of the POMPYT model this contribution can be interpreted as the remnant of the pomeron dissociation.

8 Conclusions

We have compared energy flows in ep DIS events with and without a large rapidity gap at a centre-of-mass energy of 296 GeV as a function of Q^2 for values of Q^2 above 10 GeV^2. The distributions are corrected for effects of detector acceptance and resolution. We find that the energy flows are strikingly different in the two classes of events.

In the HERA frame a clear peak in the QPM struck quark direction is observed in the non-rapidity-gap events at high values of Q^2 ($< Q^2 >= 380$ GeV^2). As Q^2 decreases this peak becomes less pronounced with most of the energy emitted at positive values of $\Delta\eta$. Substantial energy flow between the struck quark and the proton directions is observed forming an intermediate plateau the level of which depends only weakly on Q^2. In addition, the QPM peak is shifted from its direction in the naïve QPM by up to 0.4 units of pseudorapidity towards the proton direction in the lowest Q^2 bin. These features are understood as the result of QCD radiation. In the large-rapidity-gap events the energy is collimated within ± 1 unit of pseudorapidity around the QPM direction in the HERA frame. This collimation changes slowly with Q^2. Only a small shift of the QPM peak is observed even in the lowest Q^2 bin. Furthermore, there is little energy flow between the QPM struck quark and the proton directions. This strongly suggests that QCD radiation is suppressed in these events. In events selected by requiring no energy at pseudorapidities $\eta > 1.5$ we observe little energy already at pseudorapidities $\eta > -0.5$.

In the Breit frame for non-rapidity-gap events the energy flow is rising rapidly from the current towards the target region. This behaviour is well described by the CDMBGF Monte Carlo model. For the large-rapidity-gap events the energy flow is approximately constant at about 1 GeV per unit of pseudorapidity in the current and the target regions. Comparing the large-rapidity-gap events to two different models of diffractive dissociation, namely the POMPYT Monte Carlo with a hard quark density and the model by Nikolaev and Zakharov, we find that both give an adequate description of the data.

In conclusion, we have demonstrated that QCD radiation is strongly suppressed in deep inelastic scattering events with a large rapidity gap. In conjunction with our previous observation that these large rapidity gap events are consistent with a leading twist behaviour, the suppression of QCD radiation indicates the presence of a colourless object in the proton.

9 Acknowledgements

We thank Professors T. Walsh and E. Levin for valuable discussions. The strong support and encouragement by the DESY Directorate Prof. B. H. Wiik, Drs. H. Krech, J. May, Profs. P. Söding, V. Soergel, G.A. Voss and A. Wagner have been invaluable, as well as the support by Dr. G. Söhngen.

The experiment was made possible by the inventiveness and diligent efforts of the HERA machine group who continued to run HERA most efficiently during 1993.

The design, construction, and installation of the ZEUS detector have been made possible by the ingenuity and dedicated efforts of many people from inside DESY and from the home institutes who are not listed here. Their contributions are acknowledged with great appreciation.

We also gratefully acknowledge the support of the DESY computing and network services.

References

[1] ZEUS Collab., M. Derrick et al., Phys. Lett. B315 (1993) 481.

[2] B. Andersson et al., Phys. Rep. 97 (1983) 31.

[3] B. Andersson, G. Gustafson and T. Sjöstrand, Phys. Lett. B94 (1980) 211;
B. R. Webber, Nucl. Phys. B238 (1984) 492;
Ya. I. Azimov, Yu. L. Dokshitzer, V. A. Khoze, and S. I. Troyan,Phys. Lett. B165 (1985) 147.

[4] ZEUS Collab., M. Derrick et al., DESY 94–063, accepted for publication in Phys. Lett. B (1994).

[5] Ya. I. Azimov, Yu. L. Dokshitzer, V. A. Khoze and S. I. Troyan, Zeit. Phys. C27 (1985) 65.

[6] ZEUS Collab., M. Derrick et al., Z. Phys. C59 (1993) 231.

[7] The ZEUS Detector, Status Report 1993, DESY 1993.

[8] ZEUS Collab., M. Derrick et al., Phys. Lett. B 293 (1992) 465.

[9] C. Alvisi et al., Nucl. Instr. and Meth. A305 (1991) 30.

[10] C. B. Brooks et al., Nucl. Instr. and Meth. A283 (1989) 477;
B. Foster et al., Nucl. Instr. and Meth. A338 (1994) 254.

[11] A. Andresen et al., Nucl. Inst. and Meth. A309 (1991) 101.

[12] A. Bernstein et al., Nucl. Inst. and Meth. A336 (1993) 23.

[13] A. Caldwell et al., Nucl. Inst. and Meth. A321 (1992) 356.

[14] J. Andruszków et al., DESY 92–066 (1992).

[15] S. Bentvelsen, J. Engelen, and P. Kooijman, Proc. of the Workshop on Physics at HERA, Vol. 1, DESY (1991) 23, ed. W. Buchmüller and G. Ingelman.

[16] F. Jacquet and A. Blondel, in Proceedings of the study for an ep facility in Europe 79/48 (1979) 391, ed. U. Amaldi.

[17] ZEUS Collab., M. Derrick et al., Phys. Lett. B316 (1993) 412.

[18] H1 Collab.: A. De Roeck, invited talk at the Europhysics Conf. on HEP, Marseille 1993, DESY 94-005;
J. B. Dainton, invited talk at the XVI International Symposium on Lepton-Photon Interactions, Cornell 1993, RAL-94-012.

[19] G. Ingelman, Proc. of the Workshop on Physics at HERA, Vol. 3 (1991) 1366, ed. W. Buchmüller and G. Ingelman;
M. Bengtsson, G. Ingelman and T. Sjöstrand, Nucl. Phys. B301 (1988) 554.

[20] L. Lönnblad, Lund preprint, LU TP-89-10;
L. Lönnblad, Comp. Phys. Comm. 71(1992) 15.

[21] T. Sjöstrand, Comp. Phys. Comm. 39 (1986) 347; T. Sjöstrand and M. Bengtsson, Comp. Phys. Comm. 43 (1987) 367.

[22] A. Kwiatkowski, H. Spiesberger and H.-J. Möhring, Proc. of the Workshop on Physics at HERA, Vol. 3, DESY (1991) 1294, ed. W. Buchmüller and G. Ingelman.

[23] K. Charchuła, G. Schuler, H. Spiesberger, CERN–TH.7133/94.

[24] A. D. Martin, W. J. Stirling and R. G. Roberts, Phys. Lett. B306 (1993) 145.

[25] H1 Collab., I. Abt et al., Nucl. Phys. B407 (1993) 515.

[26] P. Bruni and G. Ingelman, DESY 93-187, to be publ. in Proc. of the Europhysics Conf., Marseille (1993).

[27] H.-U. Bengtsson and T. Sjöstrand, Comp. Phys. Comm. 46 (1987) 43;
T. Sjöstrand, CERN-TH.6488/92.

[28] A. Donnachie and P.V. Landshoff, Phys. Lett. 191B (1987) 309.

[29] N.N. Nikolaev and B.G. Zakharov, Z. Phys. C53 (1992) 331.

[30] A Solano, Ph. D. Thesis, University of Torino 1993, unpublished.

[31] R. Brun et al., GEANT3, CERN DD/EE/84-1 (1987).

[32] G. Marchesini and B. R. Webber, Nucl. Phys. B310 (1988) 461.

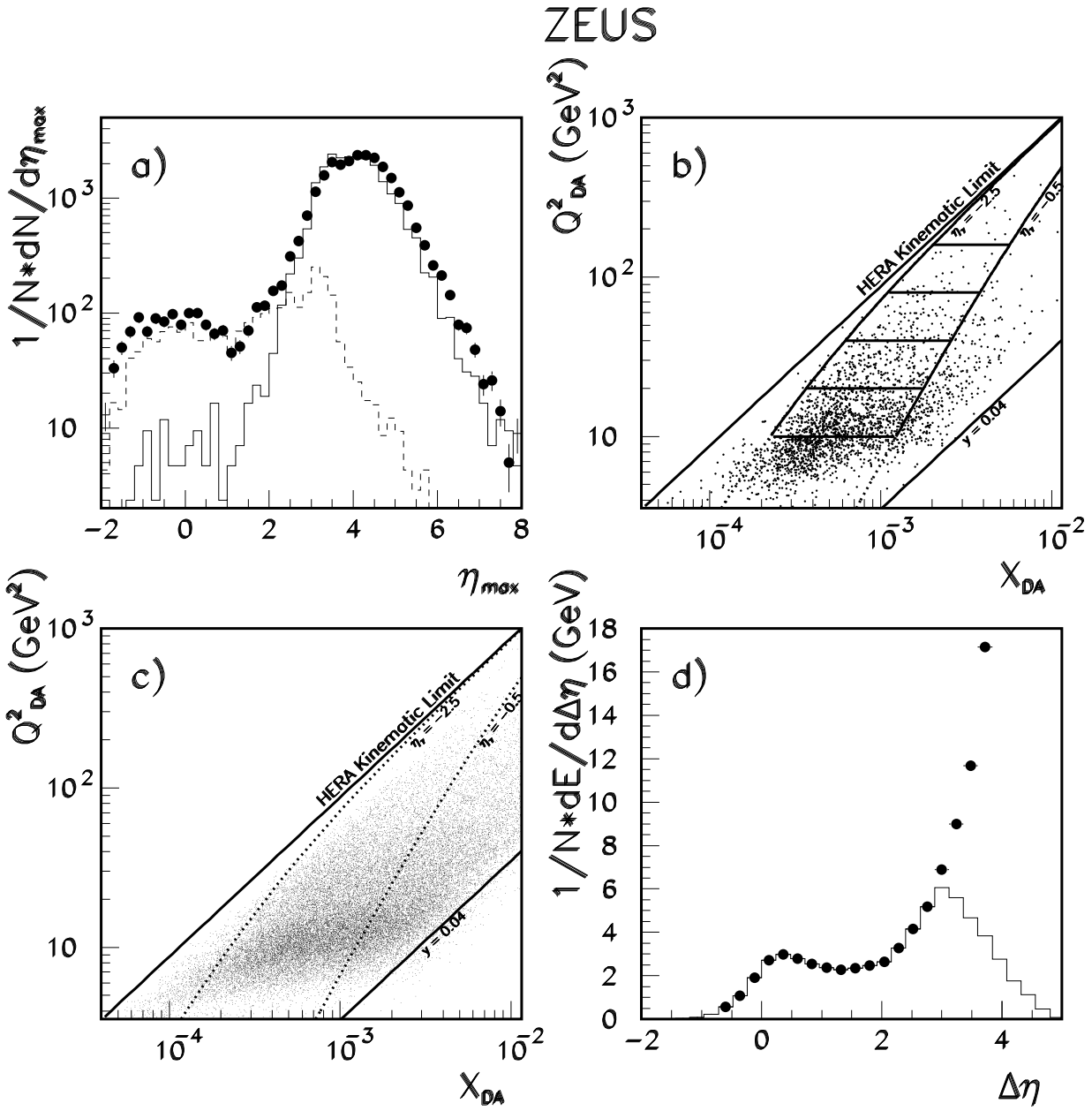

Figure 1: All distributions in this figure are uncorrected for detector acceptance and resolution.
(a): The distribution of the variable η_{max}, the rapidity of the most forward energy deposit above 400 MeV in the calorimeter. The solid circles are the ZEUS data points, the full histogram is the result of the CDMBGF Monte Carlo simulation and the dashed histogram is that of the POMPYT Monte Carlo.
(b): The distribution in the (x_{DA}, Q^2_{DA}) plane of the large-rapidity-gap events. The two curves are lines of constant γ_H, $\gamma_H = 117.5^o$ and $\gamma_H = 170.6^o$, corresponding to values of $\eta_{\gamma_H} = -0.5$ and $\eta_{\gamma_H} = -2.5$. The horizontal lines delimit the five Q^2_{DA} bins used in the analysis. The largest Q^2_{DA} bin is not bounded from above.
(c): The distribution in the (x_{DA}, Q^2_{DA}) plane of the non-rapidity-gap events.
(d): The energy flow in the HERA frame as a function of the pseudorapidity difference $\Delta\eta = \eta_{cell} - \eta_{\gamma_H}$ with and without a cut on forward energy deposits in the calorimeter. The solid circles depict the energy flow including forward energy deposits while the histogram represents the same events after those energy deposits below 10^o have been removed.

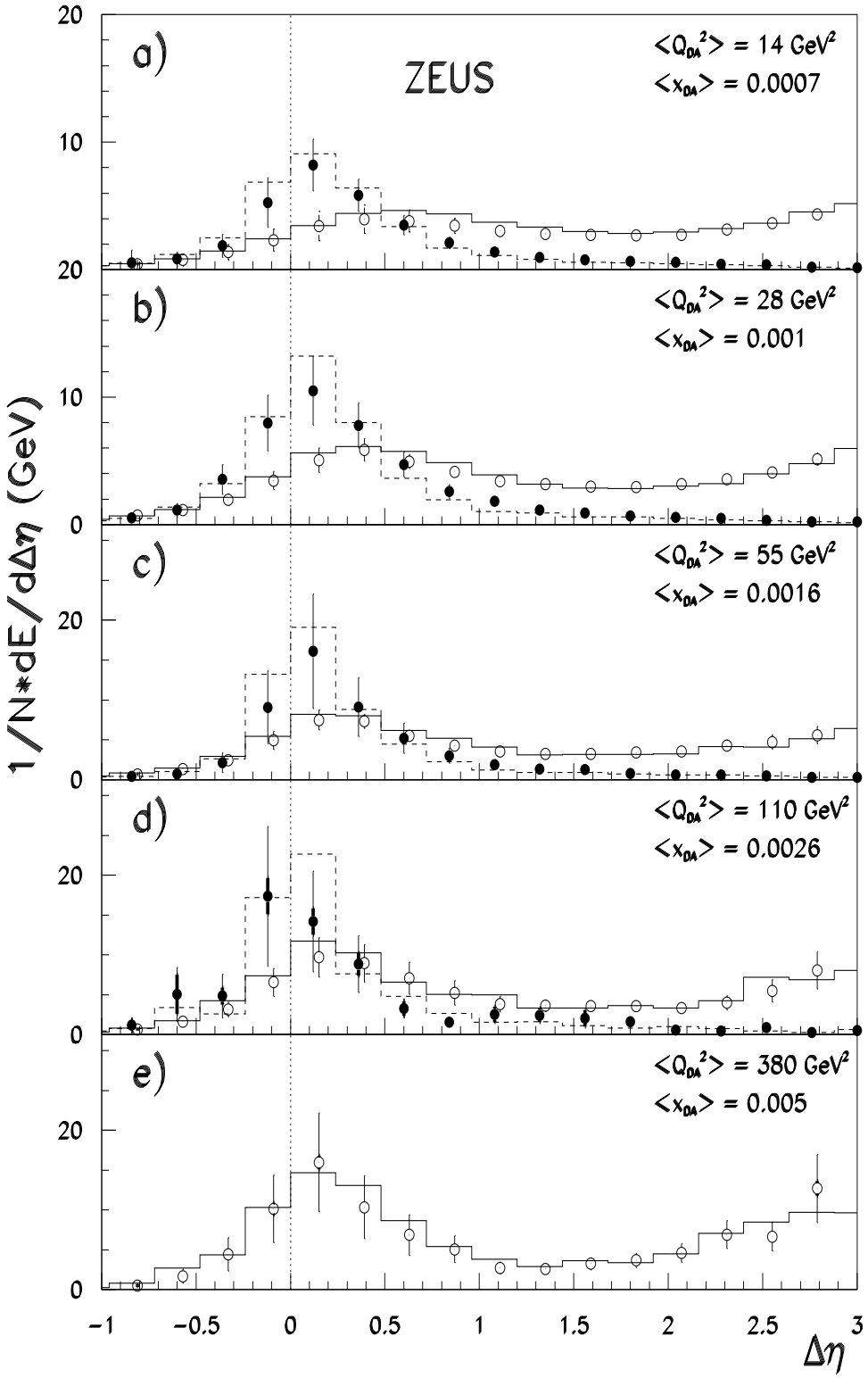

Figure 2: The energy flow distribution, $1/N \cdot dE/d(\Delta\eta)$, as a function of the pseudorapidity difference $\Delta\eta$ in five bins of Q^2_{DA}. The open circles are the non-rapidity-gap events ($\eta_{max} > 1.5$), the solid circles are the large-rapidity-gap-events, the full histogram is the expectation from the Colour Dipole Model (CDMBGF) and the dotted histogram from the POMPYT Monte Carlo. (In the highest Q^2_{DA} bin the large-rapidity-gap events are too few to be shown.) Statistical errors are shown as the thick error bars and the systematic errors are shown as the thin error bars. The large-rapidity-gap events have not been corrected for the η_{max} cut used to select these events.

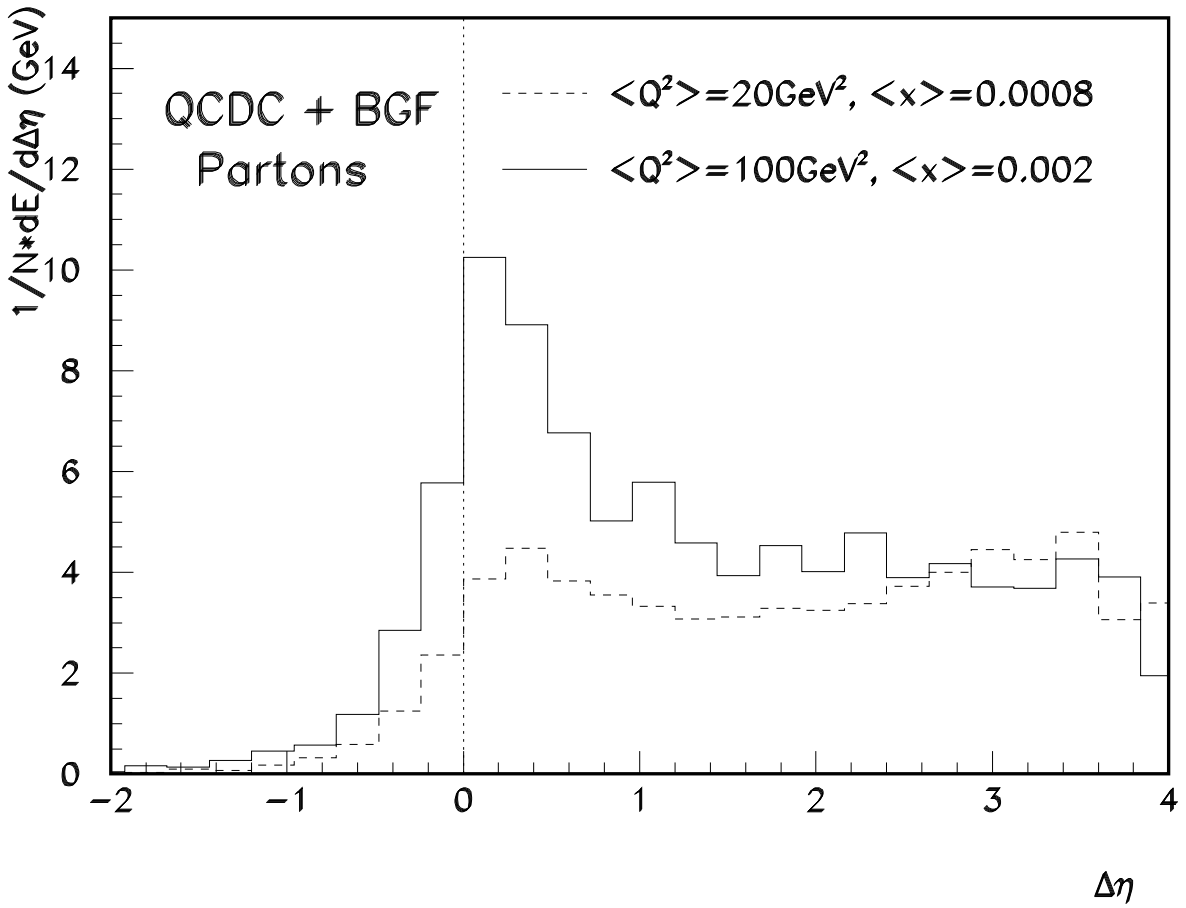

Figure 3: The distribution of the energy flow, $1/N \cdot dE/d(\Delta\eta)$, of partons as a function of the pseudorapidity difference $\Delta\eta$ in two bins of Q^2. This energy flow was produced from the first order QCD processes only, QCD Compton (QCDC) and Boson-Gluon Fusion (BGF), with the LEPTO Monte Carlo program without fragmentation. The cutoff, y_{cut}, that regulates the singularities of the matrix element was chosen at 0.0025.

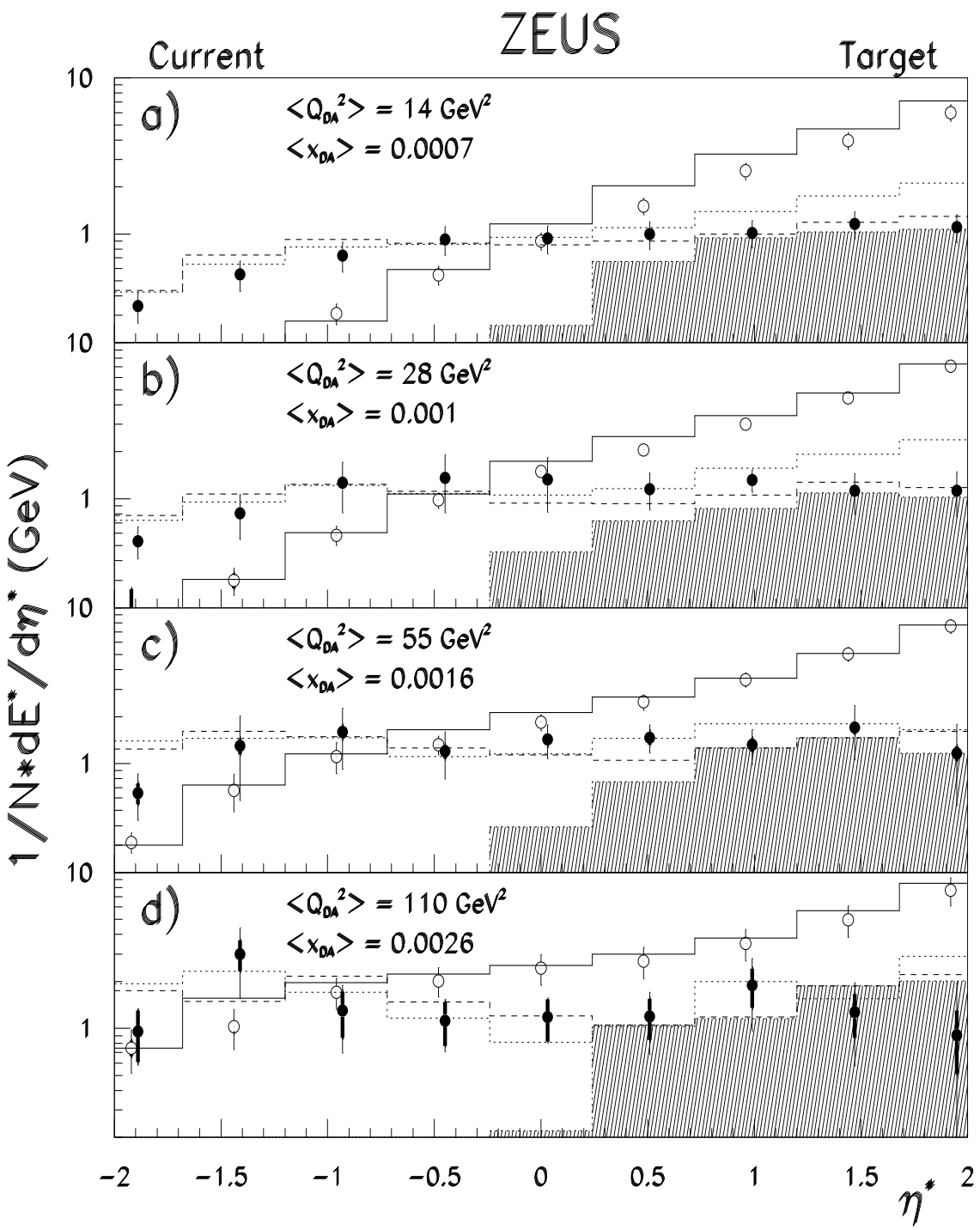

Figure 4: The energy flow distributions, $1/N \cdot dE/d\eta^\star$, as a function of the pseudorapidity in the Breit frame $\eta^\star$ in four bins of Q^2_{DA}. The open circles are the non-rapidity-gap events, the solid circles are the large-rapidity-gap events and the full histogram is the CDMBGF which should be compared to the non-rapidity-gap data. The dashed histogram is the POMPYT Monte Carlo with the hard structure function (Eq. 12) and the dotted histogram is the NZ model. The latter two models should be compared to the large-rapidity-gap data. The shaded histogram is the contribution from the target hemisphere of the centre-of-mass system of the diffractively produced hadrons as calculated in the POMPYT Monte Carlo model. Statistical errors are shown as the thick error bars and the systematic errors are shown as the thin error bars. The large-rapidity-gap events have not been corrected for the η_{max} cut used to select these events.